Eigen and Zundel Forms of Small Protonated Water Clusters: Structures and Infrared Spectra

Mina Park, Ilgyou Shin, N. Jiten Singh, and Kwang S. Kim*

Center for Superfunctional Materials, Department of Chemistry, Pohang University of Science and Technology, San 31, Hyojadong, Namgu, Pohang 790-784, Korea

Received: May 21, 2007; In Final Form: July 14, 2007

The spectral properties of protonated water clusters, especially the difference between Eigen (H_3O^+) and Zundel ($H_5O_2^+$) conformers and the difference between their unhydrated and dominant hydrated forms are investigated with the first principles molecular dynamics simulations as well as with the high level ab initio calculations. The vibrational modes of the excess proton in H_3O^+ are sensitive to the hydration, while those in $H_5O_2^+$ are sensitive to the messenger atom such as Ar (which was assumed to be weakly bound to the water cluster during acquisitions of experimental spectra). The spectral feature around ∼2700 cm^{-1} (experimental value: 2665 cm^{-1}) for the Eigen moiety appears when H_3O^+ is hydrated. This feature corresponds to the hydrating water interacting with H_3O^+, so it cannot appear in the Eigen core. Thus, H_3O^+ alone would be somewhat different from the Eigen forms in water. For the Zundel form (in particular, $H_5O_2^+$), there have been some differences in spectral features among different experiments as well as between experiments and theory. When an Ar messenger atom is introduced at a specific temperature corresponding to the experimental condition, the calculated vibrational spectra for $H_5O_2^+$·Ar are in good agreement with the experimental infrared spectra showing the characteristic Zundel frequency at ∼1770 cm^{-1}. Thus, the effect of hydration, messenger atom Ar, and temperature are crucial to elucidating the nature of vibrational spectra of Eigen and Zundel forms and to assigning the vibrational modes of small protonated water clusters.

I. Introduction

Understanding the nature of the excess proton in water is essential for elucidating the large mobility of the proton in water, the acid−base chemistry in solution, and the proton transport in membrane channels.[1] Consequently, the nature of the excess proton has been extensively investigated in both condensed phase and molecular clusters during the past few decades.[2−4] Unlike the O−H stretching of free water molecules, it has been challenging experimentally to detect the vibration modes associated with the proton, because they occur in the low-energy region where it is hard to access in the earlier experimental techniques.[5−9] Despite recent observations of the vibrational spectra involved with the proton motion, the origin of such spectra is not clear because the corresponding theoretical calculations have not properly reproduced the experimental data due to the extremely anharmonic potential surfaces of the systems. Although ab initio calculations have been useful for spectral analysis of clusters,[10] it has shown serious limitations to the study of the excess proton in water clusters even with perturbational anharmonic corrections, because the accurate description of highly anharmonic potential surfaces is practically not feasible. Hence, for such proton-mediated highly anharmonic potentials, first principles Car−Parrinello molecular dynamics (CPMD) simulations[11] have been considered to be very useful to study proton motions such as fluctuation between two limiting forms H_3O^+ (Eigen)[12] and $H_2O\cdots H^+\cdots H_2O$ (Zundel).[13] From the previous study of magic $H^+(H_2O)_{21}$ and antimagic $H^+(H_2O)_{22}$ clusters with "on the fly" CPMD simulations,[4] we have found that the results realistically match the experimental observation.[9] Such a simulation method provides important information about the structural and dynamical interpretation for protonated water species.

In this regard, we have carried out both high level ab initio calculations and first principles CPMD simulations for the H_3O^+ [$H^+(H_2O)$], $H_5O_2^+$ [$H^+(H_2O)_2$], $H_5O_2^+$·Ar [$H^+(H_2O)_2$·Ar], $H_3O^+(H_2O)_3$ [$H^+(H_2O)_4$], and $H_5O_2^+(H_2O)_4$ [$H^+(H_2O)_6$] clusters. By simulating two limiting forms, H_3O^+ and $H_5O_2^+$, and their dominant hydrated forms, $H_3O^+(H_2O)_3$ and $H_5O_2^+(H_2O)_4$, we identify the characteristic bands of Eigen or Zundel forms and the hydration effects on the infrared (IR) spectra. Besides, by performing simulations at different temperatures (50/100/150 K) we investigate the thermal and dynamic effects on the vibrational spectra. We also compare $H_5O_2^+$·Ar with $H_5O_2^+$ and explain the effect of the Ar messenger atom matrix on spectral features. We indeed find that the vibrational spectrum of Ar-tagged conformer shows a much better agreement with the Ar predissociation IR spectrum of the small protonated water clusters recently reported by Headrick et al.[5] Thus, the present paper analyzes the structures and spectra of the small protonated water clusters, discusses the effects of hydration, messenger atom Ar, and temperature, and elucidates the characteristic features of the Eigen and Zundel forms and these differences.

II. Computational Methods

We have carried out a series of geometry optimization, frequency analysis, and CPMD simulations on small protonated water clusters. Geometry optimization and harmonic/anharmonic normal mode calculations were carried out using density functional theory (DFT) with the Becke−Lee−Yang−Parr (BLYP) functionals[14] and the corresponding Becke three parameters (B3LYP) and Moller−Plesset second-order perturba-

* Corresponding author. E-mail: kim@postech.ac.kr.

10.1021/jp073912x CCC: $37.00
Published on Web 10/02/2007

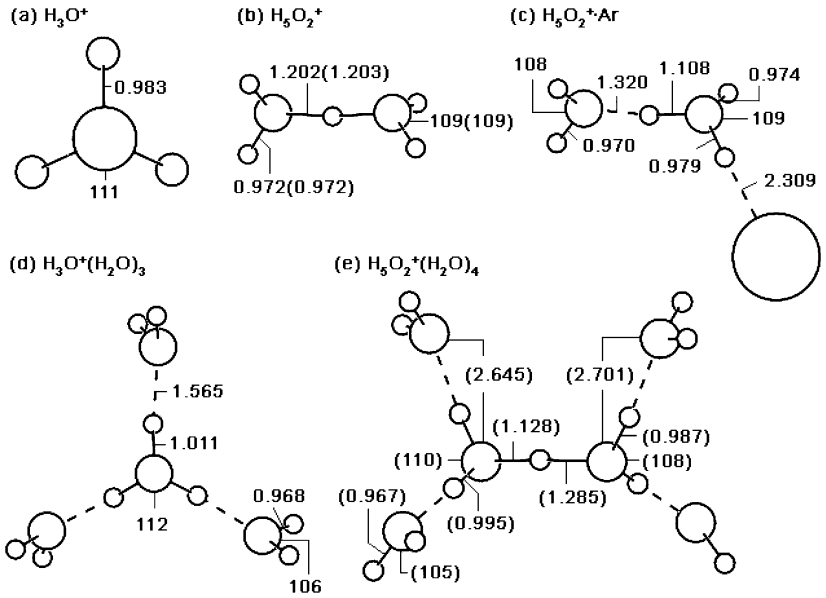

Figure 1. Ab initio optimized geometries of H_3O^+, $H_5O_2^+$, $H_5O_2^+$·Ar, $H_3O^+(H_2O)_3$, and $H_5O_2^+(H_2O)_4$ at the CCSD(T)/aVDZ (MP2/aVDZ) levels of theory.

tion theory (MP2) with the aug-cc-pVDZ and aug-cc-pVTZ basis sets (which will be abbreviated as aVDZ and aVTZ, respectively) using the Gaussian 03 suite of programs.[15] Anharmonic calculations were carried out using the correlation-corrected vibrational self-consistent field (CC−VSCF) method.[16] Calculations of the coupled cluster theory with singles, doubles, and perturbative triple excitations (CCSD(T)) using the aVDZ basis set were performed with the MOLPRO 2002 package.[17] The molecular structures were drawn with the Pohang SciTech Molecular Modeling (POSMOL) program.[18]

We also carried out the first principles CPMD simulations for 10 ps at 50, 100, and 150 K, using the CPMD code (version 3.9.2).[11] These simulations were carried out using the BLYP functionals. Poisson solver using the Tuckerman method on the reciprocal space was applied.[19] The core−valence interaction was described by a norm-conserving Trouiller−Martins pseudopotential.[20] Valence wave functions were expanded in a plane wave basis set with an energy cutoff value of 90 Ry, which is greater than the normally used value of 70 Ry for the excess proton.[4] A fictitious electron mass of 600 au and an integration step of $\Delta t = 4.135$ au (0.1 fs) were used in all of the simulations. A Nosé−Hoover thermostat[21] was attached to every degree of freedom to ensure proper thermalization over the CPMD trajectory. During the simulations, we kept the molecules at the center of an isolated cubic box of side length $L = 10$ Å for H_3O^+, $L = 16$ Å for $H_5O_2^+$, $H_5O_2^+$·Ar, and $L = 18$ Å for $H_3O^+(H_2O)_3$ and $H_5O_2^+(H_2O)_4$. On the basis of the CPMD simulations at various temperatures, we evaluated the time correlation function from which we investigated the spectra of the clusters in the equilibrium state. The Fourier transform of dipole-moment/velocity autocorrelation functions (FT-DACF/FT-VACF) is carried out.

The IR absorption spectrum can be computed from FT-DACF as

$$I(\omega) = \frac{\hbar\beta}{2\pi}\omega^2 \int \mathrm{d}t e^{-i\omega t} < \mu(0)\mu(t) >$$

Here, the symbols are used to denote intensity (I), frequency (ω), Plank constant ($\hbar = h/2\pi$), inverse of Boltzmann constant multiplied by temperature ($\beta = 1/kT$), time (t), and dipole moment (μ). For computational and interpretative purposes, it is, however, more convenient to compute the autocorrelation function of the time derivative of the dipole moment

$$I(\omega) = \frac{\hbar\beta}{2\pi} \int \mathrm{d}t e^{-i\omega t} < \dot{\mu}(0)\dot{\mu}(t) >$$

as discussed by Voth and co-workers.[3b,c] Therefore, this method is employed in our calculations. Because FT-DACF provides the information about dipole moment change resulted from vibrational motions of the molecule, FT-DACF is considered to be similar to the experimental IR spectrum. As another observable related to the IR spectra, FT-VACF is often used for the frequency analysis with intensities representing the rovibrational density of states. This FT-VACF can be used for mode analysis with the motion of a few atoms involving a specific stretching/bending mode.

III. Results

A. Structural Properties. The optimized geometries of H_3O^+, $H_5O_2^+$, $H_5O_2^+$·Ar, and $H_3O^+(H_2O)_3$ at the CCSD(T)/aVDZ level and of $H_5O_2^+(H_2O)_4$ at the MP2/aVDZ level are shown in Figure 1. The radial distribution functions (RDF) of O−H, O−O, Ar−H, and Ar−O distances (g_{OH}, g_{OO}, g_{ArH}, and g_{ArO}) and the distance fluctuation of the CPMD simulations are in Figure 2. The RDF analysis was done using data from the last 8 ps trajectory.

H_3O^+, $H_5O_2^+$, and $H_5O_2^+$·Ar. As in Figures 1 and 2, the O−H distances at the CCSD(T)/aVDZ level and the CPMD simulation are 0.98 and 1.00 Å in H_3O^+, respectively, and 0.97 and 0.98 Å in $H_5O_2^+$, respectively. These O−H distances are slightly longer than the free water O−H distance of 0.96 Å.[22] The O−O distance of $H_5O_2^+$ is 2.40 Å at CCSD(T)/aVDZ, while the entropy-driven temperature effect at CPMD/BLYP increases the distance by 0.03 Å at 50/100/150 K with respect to the value at 0 K (Figure 2a). These distances are much shorter than the O−O distance of the free water dimer (2.92 Å at CCSD(T)/aVDZ and ∼2.98 Å in experiment)[22] due to the excess charge pulling the two water molecules closer. During the 150 K simulation, the shared proton moves around widely between the two O atoms (with the H−O distance of 1.1−1.35 Å), which can be noted from the second peak of g_{OH} (Figure 2e). In the case of

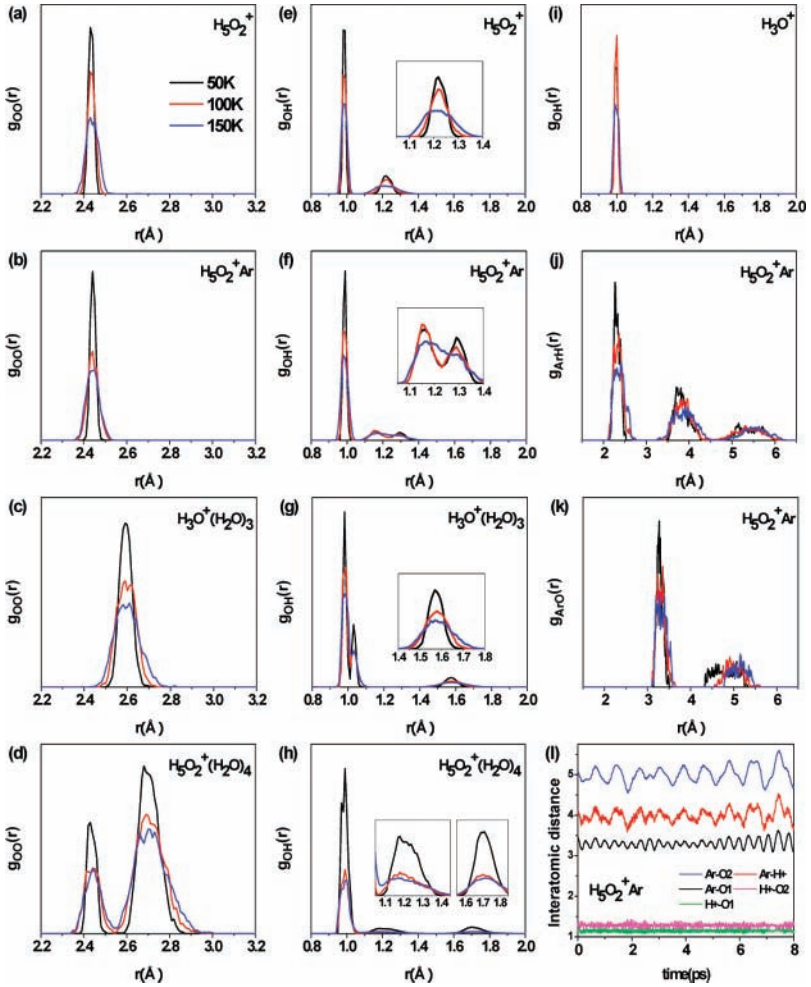

Figure 2. Radial distribution functions [g_{OO}, g_{OH}, g_{ArH}, and g_{ArO}] of the H_3O^+, $H_5O_2^+$, $H_5O_2^+$·Ar, $H_3O^+(H_2O)_3$, and $H_5O_2^+(H_2O)_4$ at 50, 100, and 150 K, and the fluctuation of the interatomic distances for the Ar−O2, Ar−H^+, Ar−O1, H^+−O2, and H^+−O1 of the $H_5O_2^+$·Ar at 100 K. (black, 50 K; red, 100 K; blue, 150 K).

$H_5O_2^+$·Ar, the O−O distance is 2.43 Å at CCSD(T)/aVDZ, 0.03 Å longer than in $H_5O_2^+$, and that for the most probable value in g_{OO} is 2.45 Å at 150 K (Figure 2b), as in $H_5O_2^+$. In contrast to the central proton in $H_5O_2^+$, Figure 1c shows that the central proton in $H_5O_2^+$·Ar shifts slightly toward the oxygen atom O1 to which the Ar atom is attached (H−O1, 1.11 Å; H−O2, 1.32 Å). Thus, although the Ar atom seems to be attached to the Zundel core H atom, it can also be considered to be attached to the Eigen core. This tendency is also found from two clearly separated peaks of the second band of g_{OH} below 100 K in Figure 2f. The distance between Ar and H is 2.31 Å at CCSD-(T)/aVDZ. The Ar atom shows slow motion, while the hydrogen atom shows fast oscillation due to their mass difference. By inspecting the fluctuation of interatomic distance between the Ar atom and the proton, the coupled motion is noted in Figure 2l.

$H_3O^+(H_2O)_3$ and $H_5O_2^+(H_2O)_4$. As in Figures 1d and 2c,g for $H_3O^+(H_2O)_3$, the O−H distance in the central Eigen core is 1.01 Å at the CCSD(T) level and ∼1.03 Å in the CPMD simulation (from the second peak of g_{OH}, while the first peak of g_{OH} appears at 0.98 Å due to the OH distances in three water molecules hydrating the Eigen core). This O−H distance in the central Eigen core is 0.03 Å longer than that in H_3O^+. Such elongation results from the O atoms of the hydrating water molecules pulling out the H atoms of the central Eigen core. In Figures 1e, and 2d,h for the central Zundel core of $H_5O_2^+(H_2O)_4$, the O−H distances between the O atoms and the noncentral H atoms are 0.99−1.00 Å, which is also ∼0.03 Å longer than that of $H_5O_2^+$. The O−O distance of the Zundel core is 2.41 Å at MP2/aVDZ (increased by only 0.01 Å compared with that in $H_5O_2^+$) and 2.44 Å at CPMD/150 K (no increase (within 0.01 Å) as compared to that in $H_5O_2^+$). Thus, the water molecules in the first hydration shell do not pull out the oxygen atoms in the central Zundel core. The O−H distance in the Zundel core is 1.13 and 1.29 Å at MP2/aVDZ, showing that the proton is not on the center of the two O atoms, in contrast to the case of bare $H_5O_2^+$. On the other hand, in the CPMD simulation, owing to the temperature effect, the g_{OH} shows the broad peak that is near the center of the two Zundel O atoms (at the O−H distance of ∼1.2 Å), while the O−H distance fluctuates between 1.1 and 1.35 Å (Figure 2g,l).

For $H_3O^+(H_2O)_3$, the O−O distance at CCSD(T)/aVDZ and that at CPMD (for the most probable value in g_{OO}) are about 2.58 and ∼2.60 Å, respectively. For $H_5O_2^+(H_2O)_4$, (when the O−O distance in the central Zundel core is excluded), the O−O distance between a Zundel O atom and its nearest hydrating water O atoms at MP2/aVDZ and that for the corresponding most probable value in g_{OO} at CPMD are 2.65∼2.70 and 2.68∼2.71 Å, respectively, which are ∼0.1 Å longer than the O−O distances in $H_3O^+(H_2O)_3$. The OH frequency related to the O−O distance (2.65∼2.70 Å) in $H_5O_2^+(H_2O)_4$ corresponds to the IR frequency of ∼3200 cm^{-1} while that related to the O−O distance (2.58 Å) in $H_3O^+(H_2O)_3$ corresponds to that of ∼2700 cm^{-1}, which will be discussed in the next section. In the case of $H_5O_2^+(H_2O)_4$, because the proton is in between two O atoms, the O−O distance of the Zundel core is shorter and

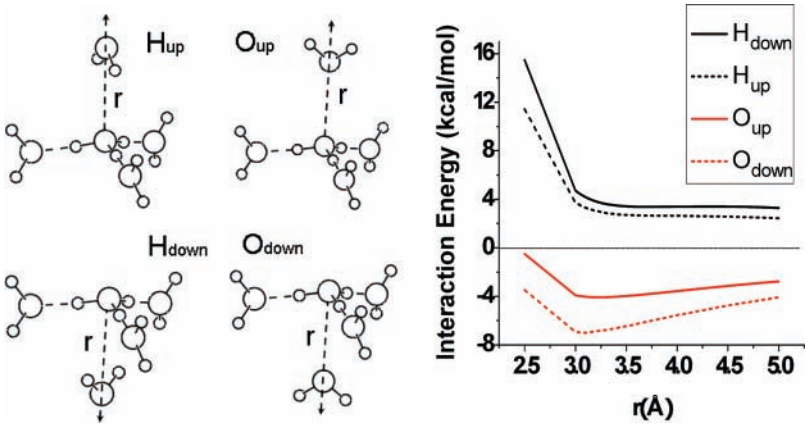

Figure 3. Geometries and interaction energies of $[H_3O^+(H_2O)_3]H_2O$ where an extra water molecule is along the *r* direction (perpendicular to the molecular cluster plane of trihydrated Eigen core) at the MP2/aVDZ level.

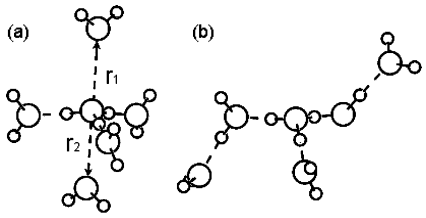

Figure 4. MP2/aVDZ optimized geometries of $H_2O[H_3O^+(H_2O)_3]H_2O$.

the non-Zundel O−O distance is longer than the O−O distance of $H_3O^+(H_2O)_3$.

Although it is clear that H_3O^+ can be easily coordinated by three water molecules by forming $H_3O^+(H_2O)_3$, one can wonder whether H_3O^+ can be able to have the coordination number up to four or five in solution or in other situations (i.e., the coordination number could be $3+\epsilon$). Thus, we investigated how many additional water molecules could be coordinated to the central Eigen core in $H_3O^+(H_2O)_3$ and which atom of such water molecules is headed to the Eigen oxygen atom. To this end, we scanned single point MP2/aVDZ energy calculations for two different conformers such that either a hydrogen or an oxygen atom of the additional water molecule is headed to the Eigen core, which were obtained by moving the additional water molecule up or down along the normal direction to the plane made by three oxygen atoms of the dangling water molecules. In Figure 3, which shows the interaction energies depending on the distance (*r*) between two oxygen atoms, we find the favorable O_{up} and O_{down} geometries. Namely, the oxygen atom of the additional water molecule above and below the plane made by three dangling water molecules around the Eigen core is headed to the Eigen core due to the attraction between the excess positive charge of the Eigen core and the dipole moment with the partial negative charge of the oxygen atom in the additional water molecule. The interaction energies between the additional water molecule and $H_3O^+(H_2O)_3$ for the O_{up} and O_{down} geometries are −4.1 and −7.0 kcal/mol at the MP2/aVDZ level, respectively; those are 16 and 27% of the interaction energy (−25.9 kcal/mol) per each hydrogen bond of the $H_3O^+(H_2O)_3$. We also carried out the MP2/aVDZ geometry optimization with two additional water molecules added to the $H_3O^+(H_2O)_3$ above and below the cluster plane. Both water molecules are 3.28 (r_1) and 3.08 (r_2) Å apart from the Eigen oxygen atom as shown in Figure 4a. The interaction energies between the two additional water molecules and the $H_3O^+(H_2O)_3$ in $H_2O[H_3O^+(H_2O)_3]H_2O$ is −11.1 kcal/mol at the MP2/aVDZ level, which is 43% of the average interaction energy for each hydrogen bond in $H_3O^+(H_2O)_3$. Therefore, we note that two additional water molecules whose oxygen atom is headed to the Eigen core can be additionally coordinated to the $H_3O^+(H_2O)_3$, and the coordination number of $H_2O[H_3O^+(H_2O)_3]H_2O$ could be roughly considered as many as 3 + 0.43 in the optimal condition. Of course, in the gas phase, the pentacoordinated Eigen structure spontaneously changes to a more stable tricoordinated Eigen structure with two additional water molecules attached to each first-hydrated water molecule, as shown in Figure 4b.

B. Vibrational Properties. We investigated the spectral features of H_3O^+, $H_5O_2^+$, $H_5O_2^+$·Ar, $H_3O^+(H_2O)_3$, and $H_5O_2^+(H_2O)_4$ (Tables 1−5) with the harmonic and anharmonic vibrational analyses of ab initio calculations and with both FT-DACF and FT-VACF of molecular dipole and atomic velocities data respectively of CPMD simulations at 50, 100, and 150 K (Figure 5). The harmonic frequencies at BLYP/aVDZ, BLYP/aVTZ, B3LYP/aVDZ, B3LYP/aVTZ, MP2/aVDZ, MP2/aVTZ, and CCSD(T)/aVDZ levels of theory were scaled by 1.001, 1.000, 0.963, 0.963, 0.957, 0.954, and 0.964, respectively, to match the average value of asymmetric and symmetric stretching frequencies of H_2O (3704 ± 55, 3706 ± 51, 3851 ± 55, 3849 ± 51, 3873 ± 67, 3885 ± 63, and 3845 ± 59 cm^{-1}, respectively) with the corresponding experimental value (3706 ± 50 cm^{-1}).[23] The effects of the messenger atom Ar and the hydration on the vibrational spectra are particularly studied. In the CPMD simulations, as the BLYP functional is known to systematically underestimate the experimental frequencies we multiplied the vibrational frequencies with scale factors. These scale factors depend on frequencies and can be changed in different systems.[24] In this study, we used the scale factor of 1.025 for H_3O^+ and $H_5O_2^+$ and the scale factor of 1.04 for hydrated/solvated Eigen and Zundel cores [$H_5O_2^+$·Ar, $H_3O^+(H_2O)_3$, and $H_5O_2^+(H_2O)_4$]. Two different scale factors are because the former is related to the O−H covalent bonds in the protonated species, while the latter involves the noncovalent hydrogen bonds (close to the typical H-bonds) related to the interaction between the H atoms of Eigen/Zundel core and the hydrating water oxygen atoms. For the Zundel system solvated by Ar, we also used the scale factor of 1.04, because the Zundel core behaves partly like an Eigen core interacting with a hydrating water molecule due to the presence of the Ar atom, which shows a partial hydrogen-bonding feature in a protonated system. In this way, the simulated spectra agree very well with the experimental data.

H_3O^+, $H_5O_2^+$, and $H_5O_2^+$·Ar. The experimental asymmetric stretching (ν_3), symmetric stretching (ν_1), and bending frequencies (ν_2) of the water monomer are 3756, 3657, and 1595 cm^{-1},

TABLE 1: Ab initio Calculated Fundamental Harmonic (ω_h) and Anharmonic (ω_a) Vibrational Frequencies (in cm^{-1}), Spectral Band Peak Positions from CPMD Simulations, and Experimental Infrared Spectra of H_3O^+[a]

	BLYP	B3LYP	MP2		CCSD(T)	CPMD	expt
mode[b]	ω_h	ω_h	ω_h	ω_a	ω_h	ω: 150 K [50 K]	w
ν_1[c]						3574_{vw}[−]	
	3529_{43}(3523)	3514_{47}(3510)	3514_{46}(3515)	3475(3506)	3537	3534_w[3544_m]	3530[d]
						3494_w[3498_m]	3514, 3490[e,f]
ν_2	3425_3(3440)	3410_3(3426)	3390_3(3411)	3368(3415)	3426	3424_{vw}[3428_w]	3390[f]
ν_3[c]	1608_9(1640)	1581_{10}(1611)	1599_9(1612)	1620(1628)	1620	1628_s[1667_m]	1639[g]
						1581_m[1616_m]	1626[g]
ν_4	810_{41}(838)	767_{44}(791)	871_{42}(861)	746(736)	889	768_s[770_s]	954,[h] 526

[a] The harmonic frequencies (ω_h) at the BLYP/aVDZ (BLYP/aVTZ), B3LYP/aVDZ (B3LYP/aVTZ), MP2/aVDZ (MP2/aVTZ), and CCSD(T)/aVDZ levels of theory were scaled by 1.001 (1.000), 0.963 (0.963), 0.957 (0.954), and 0.964, respectively, to match the average value of asymmetric and symmetric stretch frequencies of H_2O [3704 ± 55 (3706 ± 51), 3851 ± 55 (3849 ± 51), 3873 ± 67 (3885 ± 63), and 3845 ± 59, respectively] with the corresponding experimental value (3706 cm^{-1}: ref 22a). The anharmonic frequencies (ω_a) are unscaled values. Values based on the aVTZ basis set are in parentheses. IR intensities are denoted as subscripts in 10 km/mol. Band positions of MD simulation are obtained from the FT-DACF/FT-VACF at 150 K [50 K] (frequencies are scaled by 1.025). The subscripts "s', "m", "w", and "vw" beside frequencies in CPMD and expt (in other tables) denote strong, medium, weak, and very weak (or difficult to resolve), respectively. [b] ν_1(O−H asym str), ν_2(O−H sym str), ν_3(H−O−H bend), ν_4(H−O−H bend). [c] These frequencies are practically doubly degenerate for ab initio calculations but are split in CPMD simulations at finite temperatures. [d] Ref 25a. [e] Ref 25b. [f] Ref 8d. [g] Ref 25c. [h] Two frequency modes due to the tunneling splitting: ref 25d.

TABLE 2: Ab initio Calculated Fundamental Harmonic (ω_h) and Anharmonic (ω_a) Vibrational Frequencies (in cm^{-1}), Spectral Band Peak Positions from CPMD Simulations, and Experimental Infrared Spectra of $H_5O_2^+$[a]

	BLYP	B3LYP	MP2		CCSD(T)	CPMD	expt
mode[b]	ω_h	ω_h	ω_h	ω_a	ω_h	ω: 150 K [50 K]	w
ν_1	3684_{27}(3674)	3673_{28}(3664)	3669_{30}(3661)	3641(3663)	3683	3719_w[3677_m]	3695,[c] 3693,[d] 3684[e]
							3662,[d] 3660[c]
ν_2	$3594_{0.6}$(3596)	$3585_{0.9}$(3587)	$3567_{0.9}$(3569)	3552(3583)	3592 3585	− [3599_m]	3617,[d] 3615,[c] 3609[e]
	3587_{20}(3588)	3577_{23}(3579)	3560_{24}(3562)	3544(3575)		3538_s[3547_{vw}]	3528,[d] 3520[c]
ν_3	1693_{102}(1702)	1668_{111}(1678)	1672_{88}(1680)	1829(1849)	1690	1720_s[1702_s]	1756,[f] 1741[g]
	$1625_{0.0}$(1647)	$1599_{0.0}$(1619)	$1619_{0.0}$(1627)	1576(1409)	1643		
ν_4	1448_9(1478)	1430_{10}(1455)	1461_{10}(1478)	1345(1406)	1484		
						− [1407-1444_w]	1337,[f] 1317[g]
ν_5	1393_{25}(1408)	1381_{23}(1397)	1401_{26}(1405)	1309(1348)	1420		
ν_6						1014_{vw}[989_{vw}]	1163,[f] 1043[g]
	974_{261}(983)	874_{271}(891)	774_{290}(868)	545(873)	722	979_s[940_m]	990,[f] 921[g]
						887_{vw}[892_w]	788[g]

[a] See footnote *a* of Table 1. [b] ν_1(O−H asym str), ν_2(O−H sym str), ν_3(H−O−H bend), ν_4(O−H$^+$−O*y* bend), ν_5(O−H$^+$-O*x* bend), ν_6(O−H$^+$−O asym str). In most cases, the CPMD mode analysis was not needed because the DFT and ab initio modes are already available. When the BLYP/0 K and CPMD/150 K frequencies are significantly different, we used the DACF and VACF analyses, for example, for the O−H−O stretching and bending modes. The OHO bending modes (ν_4 and ν_5) are coupled in CPMD simulations. The OHO asymmetric stretch (ν_6) assignment has been made using the VACF analysis for the three atoms involving the O−H−O stretching modes, O−H−O bending modes, and the stretching−bending combined O−H−O modes. The three frequencies split around 1000 cm^{-1} are found to be mainly asymmetric (H_2)O−H−O(H_2) stretching modes, while the splitting would be due partly to the constructive, destructive, and insignificant interferences to the O−H−O asymmetric stretching mode by the H atoms of the water molecules. [c] Ref 5 for $H_5O_2^+$·Ar. [d] Ref 8c for $H_5O_2^+$·H_2. [e] Ref 8b. [f] Ref 7. [g] Ref 6.

TABLE 3: Ab Initio Calculated Fundamental Harmonic (ω_h) and Anharmonic (ω_a) Vibrational Frequencies (in cm^{-1}), Spectral Band Peak Positions from CPMD Simulations, and Experimental Infrared Spectra of $H_5O_2^+$·Ar[a]

	BLYP	B3LYP	MP2		CCSD(T)	CPMD[c]	CPMD[d]	expt[e]
mode[b]	ω_h	ω_h	ω_h	ω_a	ω_h	ω: 150 K [50 K]	ω: 150 K [50 K]	w
ν_1	3704_{22}(3692)	3630_{25}(3686)	3692_{24}(3683)	3636(3663)	3711	3642_s[3658_s]	3695_s[3712_s]	3695_s
	3637_{26}(3632)	3582_{31}(3622)	3615_{37}(3613)	3635(3645)	3628	3611_{vw}[−]	3664_{vw}[−]	3660_s
ν_2	3608_9(3608)	3543_{11}(3602)	3584_{10}(3585)	3597(3579)	3614	3560_{vw}[−]	3612_{vw}[−]	3615_w
	3448_{62}(3441)	3476_{59}(3458)	3484_{44}(3467)	3535(3527)	3505	3437_s[3419_s]	3487_s[3469_s]	3520_s
ν_3	1713_{130}(1717)	1726_{156}(1703)	1718_{154}(1714)	1583(1663)	1761	1727_s[1721_s]	1752_s[1746_s]	1768_s
	$1626_{0.3}$(1648)	$1670_{0.8}$(1619)	$1621_{0.8}$(1630)	1538(1637)	1645			
ν_4	1488_{12}(1516)	1539_{11}(1504)	1516_{15}(1521)	1453(1407)	1550	− [1519_{vw}]	− [1541_{vw}]	
ν_5	1344_{24}(1361)	1365_{23}(1335)	1326_{24}(1345)	1242(1111)	1327	− [1350_{vw}]	− [1370_{vw}]	
ν_6	1157_{217}(1161)	1094_{197}(1154)	1207_{197}(1195)	− (181)	1300	1091_s[1126_s]	1107_s[1142_s]	1089_s

[a] See footnote *a* of Table 1. Two very weak shoulder peaks at 925 cm^{-1} (which might be obtained from the bare $H_5O_2^+$) and 1872 cm^{-1} (with unclear origin) are not considered because of their ambiguity. [b] ν_1(O−H asym str), ν_2(O−H sym str), ν_3(H−O−H bend), ν_4(O−H$^+$−O*y* bend), ν_5(O−H$^+$−O*x* bend), ν_6(O−H$^+$-O asym str). [c] Frequencies are scaled by 1.025. [d] Frequencies are scaled by 1.04. This scale factor shows better agreement with experiments. [e] Ref 5.

respectively.[23] These results are reasonably well reproduced from ab initio calculations by using scaled harmonic frequencies or unscaled anharmonic frequencies. Here, to facilitate our discussion, for the frequency modes of protonated water clusters, we assign the highest frequency mode as ν_1, and the lower frequencies ν_n in the descending order. For H_3O^+, a few

TABLE 4: Ab Initio Calculated Fundamental Harmonic (ω_h) and Anharmonic (ω_a) Vibrational Frequencies (in cm^{-1}), Spectral Band Peak Positions from CPMD Simulations, and Experimental Infrared Spectra of $H_3O^+(H_2O)_3$[a]

	BLYP	B3LYP	MP2		CCSD(T)	CPMD	expt
mode[b]	ω_h	ω_h	ω_h	ω_a	ω_h	ω: 150 K [50 K]	w
ν_1[c]	3744_{34}(3734)	3736_{45}(3726)	3733_{43}	3716	3742	3726_m[3729_m]	3730_s,[d,e] 3710[f]
ν_2[c]	3645_6(3646)	3639_7(3639)	3619_7	3608	3642	3632_w[3634_{vw}]	3644_m,[d,e] 3620[f]
ν_3	2825_{14}(2832)	2863_{13}(2869)	2880_{17}	2710	2943	2828_m[2803_w]	
ν_4[c]	2700_{307}(2686)	2758_{304}(2743)	2811_{289}	2686	2864	2771_s[2783_s]	2665_s[d]
ν_5[c]	1633_3(1662)	1603_2(1634)	1636_1	1611	1658	1737_w[-]	1900_w,[d] 1760_m[d]
ν_6	$1591_{0.0}$(1607)	$1567_{0.0}$(1580)	$1568_{0.0}$	1600	1592	1607_w[1627_w]	1620_m[d]
ν_7[c]	1565_3(1588)	1547_4(1567)	1554_6	1580	1578		
ν_8	1127_{22}(1164)	1083_{27}(1120)	1151_{23}	987	1161	− [1108_w]	1045_w[d]
ν_9[c]	970_6(956)	949_5(934)	931_7	892	928	896_{vw}[961_{vw}]	

[a] See footnote *a* of Table 1. Frequencies from CPMD simulations are scaled by 1.04. [b] ν_1(O−H asym str of the dangling water molecules), ν_2(O−H sym str of the dangling water molecules), ν_3(O−H sym str of the Eigen moiety), ν_4(O−H asym str of the Eigen moiety), ν_5(H−O−H bend of the Eigen moiety (major component) and the dangling water molecules (minor component)), ν_6(H−O−H bend of the dangling water molecules), ν_7(H−O−H bend of the dangling water molecules and the Eigen moiety, which are almost in equivalent contribution), ν_8(H−O−H sym bend in Eigen), ν_9(H−O−H asym bend in Eigen). [c] These fundamental frequencies are practically doubly degenerate in ab initio calculations (within 1 cm^{-1} due to the near C_3 symmetry: E irreducible representation). [d] Ref 5. [e] Ref 8b. [f] Ref 8d.

TABLE 5. Ab Initio Calculated Fundamental Harmonic (ω_h) and Anharmonic (ω_a) Vibrational Frequencies (in cm^{-1}), Spectral Band Peak Positions from CPMD Simulations, and Experimental Infrared Spectrum of $H_5O_2^+(H_2O)_4$[a]

	BLYP	B3LYP	MP2	CPMD	expt[d]
mode[b]	ω_h	ω_h	ω_h	ω: 150 K [50 K]	w
ν_1[c]	3750_7(3742)	3743_{10}(3736)	3742_{12}	3723_m[3728_m]	3740_s
ν_2[c]	3650_3(3652)	3646_4(3648)	3626_4	3631_m[3636_m]	3650_m
ν_3	3184_2(3189)	3235_7(3224)	3326_{147}	3282_s[3263_s]	3250_{vw}
	3167_{154}(3163)	3187_{164}(3205)	3151_{190}		
ν_4	3170_{240}(3165)	3227_{236}(3208)	3280_{46}	3189_s[−]	
	3146_{95}(3153)	3174_{71}(3189)	3135_{77}	3145_s[3201_s]	3160_s
ν_5	1692_{59}(1707)	1671_{71}(1683)	1701_{87}	1773_s[1738_s]	1770_s
	$1652_{0.5}$(1676)	$1628_{0.5}$(1653)	$1659_{0.9}$		
ν_6[c]	1584_9(1601)	1561_8(1576)	1560_7	− [1623_m]	1620_m
ν_7	1511_4(1546)	1500_5(1533)	1539_{12}		
ν_8	1392_{16}(1410)	1371_{16}(1385)	1360_{21}		
ν_9	985_{240}(994)	943_{208}(947)	1153_{310}	1055_s[967_s]	1055_s

[a] See footnote *a* of Table 1. Frequencies from CPMD simulations are scaled by 1.04. [b] ν_1(O−H asym str in dangling water), ν_2(O−H sym str in dangling water), ν_3(O−H asym str in Zundel), ν_4(O−H sym str in Zundel), ν_5(H−O−H bend in Zundel), ν_6(H−O−H bend in dangling water), ν_7(O−H$^+$-O*y* bend), ν_8(O−H$^+$−O*x* bend), ν_9(O−H$^+$−O asym str). [c] These fundamental frequencies are practically quadruply degenerate in ab initio calculations. [d] Ref 5.

experiments[8d,25] observed a few different regions, reporting the asymmetric stretching frequencies (ν_1) around 3530 and 3514/3490 cm^{-1}, the symmetric stretching frequencies (ν_2) at 3390 cm^{-1}, the bending frequencies (ν_3) at 1639 and 1626 cm^{-1}, and another bending frequencies (ν_4) at 954 and 526 cm^{-1}. Ab initio calculations show two degenerate peaks at ν_1 and ν_3, while CPMD simulations show two (or a few) split frequencies for ν_1 and two split frequencies for ν_3 due to anharmonic couplings. For ν_1, the experimental two split peaks (3530 and 3514/3490 cm^{-1}) are in good agreement with the CPMD two split frequencies (3544 and 3498 cm^{-1} at 50 K; 3534 and 3494 cm^{-1} at 150 K; the very weak frequency 3574 cm^{-1} at 150 K does not need to be considered) and also with the degenerate ab initio frequencies (∼3500 cm^{-1}). The experimental ν_2 (3390 cm^{-1}) is in good agreement with the CPMD ν_2 (3424/3428 cm^{-1} at 150/50 K) and with the ab initio ν_2 (∼3400 cm^{-1}). The experimental two split ν_3 (1639 and 1626 cm^{-1}) are in reasonable agreement with the CPMD two split frequencies (1628/1667 and 1581/1616 cm^{-1} at 150/50 K) and with the ab initio degenerate frequencies (∼1600 cm^{-1}). For ν_4, the experiment shows two frequencies due to the tunneling splitting (954 and 526 cm^{-1}),[7] while the CPMD and ab initio calculations (∼800 cm^{-1}) did not consider such splitting.

For the clusters having the Zundel moiety, there has been a long argument about the assignment of the bridging proton oscillation mode around 1000 cm^{-1}. Regarding the protonated water dimer,[5−8] Asmis et al.[6] observed 921, 1043, 1317, and 1741 cm^{-1}; Fridgen et al.[7] assigned the bands centered at 990, 1163, 1337, and 1756 cm^{-1} to the O−H$^+$−O stretching mode and H−O−H bending mode; Headrick et al.[5] observed 1089 cm^{-1} and 1768 cm^{-1} for $H_5O_2^+$·Ar at a low temperature. These experiments show a broad band (with a few peaks) around ∼1000 cm^{-1} and a unique Zundel peak around ∼1750 cm^{-1}. A number of theoretical studies of $H_5O_2^+$ have been carried out.[26] However, the clear assignment of the Zundel form still needs to be made, as experimental values vary depending on the experimental condition. As shown in the of $H_5O_2^+$ spectra of Table 2, the O−H asymmetric stretch mode (ν_1) appears at ∼3690 and ∼3660 cm^{-1} in experiments, 3719/3677 cm^{-1} at 150/50 K simulations, and ∼3680 cm^{-1} for ab initio calculations. The O−H symmetric stretch mode (ν_2) appears at ∼3615 and ∼3525 cm^{-1} in experiments, 3599/3538 cm^{-1} in 50/150 K simulations, and ∼3590 and ∼3580 cm^{-1} in ab initio calculations. The H−O−H bending mode (ν_3) appears at ∼1750 cm^{-1} in experiments, 1720/1702 cm^{-1} in 150/50 K simulations, and ∼1690 cm^{-1} (strong intensity) in ab initio calculations, while another H−O−H bending mode (ν_3) around ∼1640 cm^{-1} in ab initio calculations shows almost zero intensity. The two O−H$^+$−O bending modes (ν_4 and ν_5) with weak intensity appear around ∼1450 and ∼1400 cm^{-1} for 50 K simulations

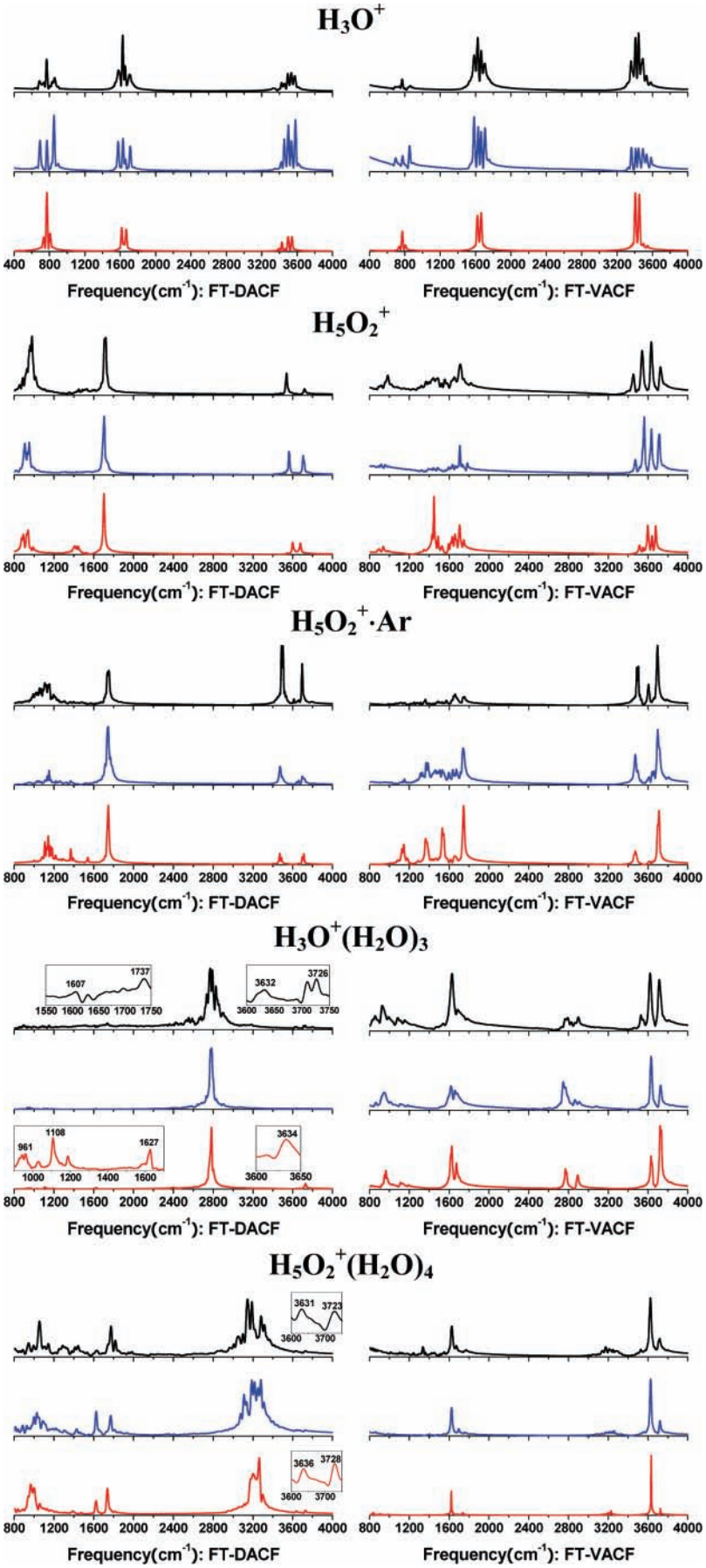

Figure 5. FT-DACF (left) and FT-VACF (right) of H_3O^+, $H_5O_2^+$, $H_5O_2^+ \cdot Ar$, $H_3O^+(H_2O)_3$, and $H_5O_2^+(H_2O)_4$ at 50, 100, and 150 K (with first/red, second/blue, and third/black lines from below, respectively).

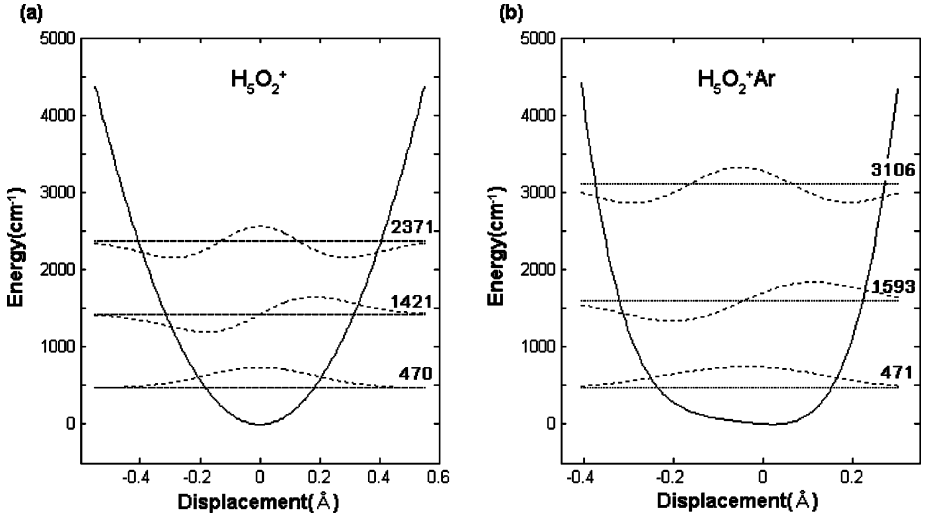

Figure 6. Potential energy curves and vibrational energy levels of (a) $H_5O_2^+$ and (b) $H_5O_2^+$·Ar

and ab initio calculations. However, above 100 K, the two peaks almost disappear. For the O−H$^+$−O asymmetric stretching mode (ν_6), ab initio calculations predict a peak around 700−1000 cm^{-1} (depending on the level of theory), and the 150 K simulation shows a peak around ∼980 cm^{-1}, while the 50 K simulation gives a medium peak around ∼940, a weak peak around ∼890, and a very weak peak around ∼990 cm^{-1}. The experimental peaks around ∼1000 cm^{-1} were observed at 788, 921, 1043, and 1317 cm^{-1} by Asmis et al. and at 990, 1163, and 1337 cm^{-1} by Fridgen et al. It is not clear to us whether the frequency of 1317/1337 cm^{-1} would correspond to the O−H$^+$−O bending modes (ν_4 and ν_5) around ∼1400 cm^{-1}. All calculations show that a broad band (with a few peaks) is around ∼950 cm^{-1} and a unique Zundel peak is around ∼1750 cm^{-1}, which agrees with experiments. The broad frequency band (with a few peaks) around ∼950 cm^{-1} is somewhat off the experimental frequency 1089 cm^{-1} observed for $H_5O_2^+$·Ar by Headrick et al. Thus, the effect of an Ar messenger atom on the $H_5O_2^+$ spectra needs to be investigated.

In the case of $H_5O_2^+$·Ar, the O−H asymmetric stretch mode (ν_1) appears with two split peaks at 3695 and 3660 cm^{-1} in experiments. These are well reproduced in the 150 K CPMD simulation, which shows two split peaks at 3695 and 3664 cm^{-1}, while ab initio calculations show a degenerate peak around ∼3700 cm^{-1}. The O−H symmetric stretch mode (ν_2) appears at 3615 and 3520 cm^{-1} in experiments, 3612 and 3487 cm^{-1} in the 150 K simulation, and ∼3600 and ∼3500 cm^{-1} in ab initio calculations. The H−O−H bending mode (ν_3) with strong intensity appears at 1768 cm^{-1} in experiments, 1752 cm^{-1} in the 150 K simulation, and ∼1700 cm^{-1} in ab initio calculations, while another weak H−O−H bending mode (ν_3) shows almost zero intensity, as can be noted from the ab initio frequency around ∼1640 cm^{-1} as well as the disappearance of such a peak in the 150 K simulation. The two O−H$^+$−O bending modes (ν_4 and ν_5) with weak intensity appear around ∼1540 and ∼1370 cm^{-1} for the 50 K simulations but disappear above 100 K. These modes appear at 1500 and 1300 cm^{-1} with weak intensity in ab initio calculations. The O−H$^+$−O asymmetric stretching mode (ν_6) appears at 1089 cm^{-1} in experiments, 1107 cm^{-1} in the 150 K simulation, and ∼1200 cm^{-1} in ab initio calculations.

Although anharmonic frequencies involving coupling between modes are properly taken into account in CPMD simulations, the scaling method in ab initio calculations is not physically sound, and the low-order anharmonic perturbation correction method is not reliable to describe the proton-oscillating mode for $H_5O_2^+$ and $H_5O_2^+$·Ar. In this regard, to correctly understand the Ar messenger effect in ab initio calculations, we must obtain accurate frequencies for the proton-oscillating asymmetric stretching mode (ν_6) for both $H_5O_2^+$ and $H_5O_2^+$·Ar. Thus, we studied the potential energy surfaces of both $H_5O_2^+$ and $H_5O_2^+$·Ar, as shown in Figure 6. The CCSD(T)/aVTZ single point energy calculations were carried out at several geometries that were obtained by moving the proton in the Zundel ion along the normal mode direction at the MP2/aVTZ optimized geometries. The potential energy curves were fitted in Taylor series, and the one-dimensional Schrödinger equation was numerically solved.[27] The calculated eigenvalues corresponding to the three lowest vibrational modes of the $H_5O_2^+$are $E_0 = 470$ and $E_1 = 1421$ cm^{-1}. Thus, the fundamental vibrational frequency of the ν_6 mode is 951 cm^{-1}, similar to the simulated frequencies (979/940 cm^{-1} 150/50 K) for $H_5O_2^+$. On the other hand, the eigenvalues of $H_5O_2^+$·Ar corresponding to the three lowest vibrational modes are $E_0 = 471$ and $E_1 = 1593$ cm^{-1}, so that the lowest vibrational frequency mode ν_6 is 1122 cm^{-1}.

From the CPMD simulations of the Ar-tagged conformer as compared to $H_5O_2^+$, the ν_1 mode is significantly blue-shifted from 979 to 1091/1107 cm^{-1} at 150 K and from 940 to 1126/1142 cm^{-1} at 50 K at the FT-DACF spectra, in agreement with experiments (from 921/990 to 1089 cm^{-1}) as well as the CCSD-(T)/aVTZ//MP2/aVTZ frequency analysis of the ν_6 mode (from 951 to 1122 cm^{-1}). From these spectral analyses, we note that the messenger atom Ar shows a significant shift in the frequency of the ν_6 mode. This is actually expected because the central proton in $H_5O_2^+$·Ar is not near the center of the two O atoms; thus, although the Ar atom seems to be attached to the Zundel core H atom, it can also be partly considered to be attached to the Eigen core, which is contrasted to the pure Zundel form of $H_5O_2^+$. The ν_3 mode is slightly blue-shifted from 1720 to 1727/1752 cm^{-1} at 150 K and from 1702 to 1721/1746 cm^{-1} at 50 K due to the Ar tagging, consistent with the experiments (from 1741/1756 to 1768 cm^{-1}). Thus, the Ar-tagging effect explains some differences in frequencies among different experimental conditions.

$H_3O^+(H_2O)_3$ and $H_5O_2^+(H_2O)_4$. In the case of $H_3O^+(H_2O)_3$, the hydration shell makes the O−H asymmetric and symmetric modes and H−O−H bending modes blue-shifted as compared with the bare H_3O^+. In addition, more complicated bending modes appear, and the characteristic O−H stretching modes of

the Eigen core appear. The O−H asymmetric and symmetric stretch modes (ν_1 and ν_2) appear at (3730/3710 and 3644/3620 cm^{-1}) in experiments, (3726/3729 and 3632/3634 cm^{-1}) at 150/50 K simulations, and (∼3740 and ∼3640 cm^{-1}) in ab initio calculations. The O−H symmetric stretch frequency (ν_3) around ∼2820 cm^{-1} (difficult to be resolved from the strong peak at ∼2771 cm^{-1}) was not observed in experiments. On the other hand, the characteristic strong O−H asymmetric stretch frequency (ν_4) at 2771/2783 cm^{-1} in 150/50 K simulations and at ∼2800 cm^{-1} in ab initio calculations was observed at 2665 cm^{-1} in experiments. The weak H−O−H bending modes (ν_5 and ν_6) appear (1760 and 1620 cm^{-1}) in experiments, (1737 and 1607/1627 cm^{-1}) in 150/50 K simulations, and (∼1650 and ∼1590 cm^{-1}) in ab initio calculations. A weak H−O−H symmetric-bending frequency (ν_8) appears at 1045 cm^{-1} in experiments, 1108 cm^{-1} in 50 K simulations, and ∼1150 cm^{-1} in ab initio calculations. Other very weak H−O−H bending modes (ν_7 at ∼1580 cm^{-1} and ν_9 at ∼900 cm^{-1}) were not observed in experiments.

In the case of $H_3O^+(H_2O)_3$, the origin of the frequencies at 1760 and 1900 cm^{-1} is not clear. It is known that the band near 1760 cm^{-1} indicates Zundel moieties, which is evidenced from such a peak at the experimental IR spectra of $H_5O_2^+$ and $H_5O_2^+(H_2O)_4$ conformers. This peak is observed near 1722 and 1744 cm^{-1} in the MD simulations of $H_5O_2^+$·Ar and $H_5O_2^+(H_2O)_4$, respectively, which will be discussed later. Thus, the experimental peak near 1760 cm^{-1} could indicate the probabilistic appearance of Zundel moiety resulted from the fluctuation of the hydrogen atoms in the Eigen core arisen from some of nonequilibrated hot clusters. Meanwhile, the experimental vibrational peak near 1900 cm^{-1} is unclear to us because they are not observed from ab initio-calculated and CPMD-simulated spectra. We do not exclude a possibility that such peaks could arise from a low-lying energy isomer that could be stable at somewhat high temperatures.

Like $H_3O^+(H_2O)_3$, in the case of $H_5O_2^+(H_2O)_4$ the hydration shell makes the O−H asymmetric and symmetric modes and H−O−H-bending modes blue-shifted as compared with the bare $H_5O_2^+$. The O−H asymmetric and symmetric stretch modes (ν_1 and ν_2) appear at (3740 and 3650 cm^{-1}) in experiments, (3723/3728 and 3631/3636 cm^{-1}) at 150/50 K simulations, and (∼3740 and ∼3640 cm^{-1}) in ab initio calculations. These outershell water molecular frequencies are almost the same with those of $H_3O^+(H_2O)_3$. The O−H asymmetric stretch frequencies (ν_3) are very weak at ∼3250 cm^{-1} in experiments, 3282/3263 in 150/50 K simulations, and ∼3200 cm^{-1} in ab initio calculations. The O−H symmetric stretch frequency (ν_4) appears strongly at 3160 cm^{-1} in experiments, 3145/3201 cm^{-1} in 150/50 K simulations, and ∼3150 cm^{-1} in ab initio calculations. The strong H−O−H bending modes of the Zundel core (ν_5) appears at 1770 cm^{-1} in experiments, 1733/1738 cm^{-1} in 150/50 K simulations, and ∼1700 cm^{-1} in ab initio calculations, while the very weak peak around ∼1650 cm^{-1} is not observed in experiments and CPMD simulations. The H−O−H bending mode (ν_6) appears 1620 cm^{-1} in experiments, 1623 cm^{-1} in 50 K simulations, and ∼1570 cm^{-1} in ab initio calculations. Very weak O−H$^+$−O-bending frequencies (ν_7 and ν_8) at ∼1510 and ∼1370 cm^{-1} in ab initio calculations are not observed in both experiments and CPMD simulations. The O−H$^+$−O asymmetric stretching frequency (ν_9) appears at 1055 cm^{-1} in experiments, 1055/967 cm^{-1} in 150/50 K simulations, and ∼1000 cm^{-1} in ab initio calculations.

On the basis of the MD simulation for $H_5O_2^+(H_2O)_4$, most vibrational modes of $H_5O_2^+$ are slightly blue-shifted except for the new O−H stretching modes of the water molecules in the central Zundel ion. At the CPMD/150 K simulations, although the intensities of the broad ν_3 (3282 cm^{-1}) and ν_4 (3145 cm^{-1}) bands are strong the intensities of both O−H asymmetric-stretching ν_1 (3723 cm^{-1}) and symmetric ν_2 (3631 cm^{-1}) modes of the free water molecules in the first hydration shell are weak (Figure 5). On the basis of our assessment of the predicted temperature-dependent spectra in terms of the overall agreements with the experimental data, we estimate the experimental temperature to be 100−150 K (for example, the O−H symmetry-stretching frequency at 150 K (3145 cm^{-1}) is close to the experimental value (3160 cm^{-1})).

As discussed above, we have observed realistic frequencies based on the CPMD simulations, which are in good agreement with experiments. Although the energy barrier of the CPMD potential tends to be lower than the more accurate ab initio results, the underestimation of the CPMD potential barriers is likely to partially reflect the quantum-tunneling driven effective barriers for the accurate potential surface and would give more realistic simulation results, as noted in our previous simulation study of the magic- and antimagic-protonated water clusters.[4]

IV. Concluding Remarks

We have investigated the spectral features of small protonated water clusters, Eigen core (H_3O^+), Zundel core ($H_5O_2^+$), Zundel core solvated by Ar ($H_5O_2^+$·Ar), hydrated Eigen core [$H_3O^+(H_2O)_3$], and hydrated Zundel core [$H_5O_2^+(H_2O)_4$]. Our special attention has been focused on the proton motions based on ab initio calculations and CPMD simulations. By comparing the bare Eigen and Zundel cores with their dominant hydrated/solvated conformers, we investigated the hydration/solvation effect on the characteristic vibrational peaks of Eigen or Zundel forms. The characteristic Eigen frequency (H−O−H bending between the OH of hydrating water molecules and the H atom in Eigen core) is ∼2700 cm^{-1}, which arises from the interaction between the Eigen core and the hydrating water molecules. Thus, this unique feature cannot be seen for the Eigen core alone. One can easily note that the coordination number of the Eigen core has clearly three in the gas phase, but it could be increased up to ∼3.4 when it is fully hydrated, because the O atoms of the additional hydrating water molecules above and below the molecular cluster plane of trihydrated Eigen core are likely to be headed to the positively charged Eigen core.

From the study of $H_5O_2^+$ and $H_5O_2^+$·Ar clusters, we find the significant effect of the messenger atom Ar on the proton position/motion and the relevant vibrational frequency. In the Zundel core solvated by the messenger atom Ar, the central proton shifts its position toward to the O atom to which the Ar atom is attached, resulting in breaking the quasi-C_2 symmetry of the bare $H_5O_2^+$ structure. Thus, both ab initio-calculated and CPMD-simulated vibrational spectra of the Ar-tagged conformer $H_5O_2^+$·Ar are significantly different from those of the bare $H_5O_2^+$. For the CPMD simulations of the Ar-tagged conformer, the O−H$^+$−O asymmetric stretch mode is significantly blue-shifted from 979 to 1091/1107 cm^{-1} at 150 K, which is in agreement with experiments (from 921/990 to 1089 cm^{-1}). This shift can be also understood from the anharmonicity-driven vibrational frequency change (951 to 1122 cm^{-1}) based on the CCSD(T)/aVTZ//MP2/aVTZ potential energy surface. The unique Zundel frequency (H−O−H bending mode) is ∼1750 cm^{-1}. By Ar-tagging, this frequency is slightly blue-shifted (from 1720 to 1727/1752 cm^{-1} at the CPMD/150 K simulation), which is consistent with experiments (from 1741/1756 to 1768 cm^{-1}). Thus, the significant effect of an Ar messenger atom on

the $H_5O_2^+$ spectra around ~1000 and ~1750 cm^{-1} is due to the structural change from the pure Zundel form of $H_5O_2^+$ to the Zundel−Eigen hybrid form of $H_5O_2^+$·Ar by the symmetry breaking of the structure in the presence of an Ar atom. As the potential surface with respect to the proton motion is highly anharmonic, the temperature effect is also not small on the spectra. All these effects explain the differences in spectra among different experimental conditions. The spectrum of $H_5O_2^+$ without Ar matches well with the experimental results of Asmis et al. and Fridgen et al. while that with a tagged Ar matches well with the experimental results of Headrick et al.[5−7]

The O−H stretching vibrational modes of the Eigen and Zundel cores are generally blue-shifted in their hydrated clusters due to the interaction with the hydrating water molecules. As the temperature increases, some peaks are either broadened or disappeared. To sum up, by taking into account the effects of hydration, messenger Ar atom, and temperature, we were able to realistically reproduce the experimental IR spectra and elucidate the nature of the characteristic features of Eigen and Zundel forms except for very few unclearly resolved experimental frequencies.

Acknowledgment. This paper has been dedicated to Prof. Fumio Hirata, who has been a long-time friend of mine, for his 60th birthday. This work was supported by the Brain Korea 21 program and Global Research Laboratory (GRL) program of KICOS. Most calculations were performed with supercomputers at KISTI.

Supporting Information Available: The unscaled frequencies of Tables 1−5. This material is available free of charge via the Internet at http://pubs.acs.org.

References and Notes

(1) (a) Kornyshev, A. A.; Kuznetsov, A. M.; Spohr, E.; Ulstrup, J. *J. Phys. Chem. B* **2003**, *107*, 3351. (b) Duff, K. D.; Ashley, R. H. *Virology* **1992**, *190*, 485. (c) Pomes, R.; Roux, B. *J. Phys. Chem.* **1996**, *100*, 2519.

(2) (a) Geissler, P. L.; Dellago, C.; Chandler, D.; Hutter, J.; Parrinello, M. *Science* **2001**, *291*, 2121. (b) Marx, D.; Tuckermann, M. E.; Hutter, J.; Parrinello, M. *Nature* **1999**, *397*, 601. (c) Tuckerman, M. E.; Marx, D.; Klein, M. L.; Parrinello, M. *Nature* **1997**, *275*, 817.

(3) (a) Wei, D.; Salahub, D. R. *J. Chem. Phys.* **1997**, *106*, 6086. (b) Schmitt, U. W.; Voth, G. A. *J. Chem. Phys*. **1999**, *111*, 9361. (c) Kim, J.; Schmitt, U. W.; Gruetzmacher, J. A.; Voth, G. A.; Scherer, N. E. *J. Chem. Phys*. **1999**, *111*, 9361. (d) Mella, M.; Clary, D. C. *J. Chem. Phys.* **2003**, *119*, 10048. (e) Iyengar, S. S.; Petersen, M.; Day, T. J. F.; Burnham, C. J.; Teige, V. E.; Voth, G. A. *J. Chem. Phys*. **2005**, *123*, 084309. (f) Lee, H. M.; Tarakeshwar, P.; Park, J. W.; Kolaski, M. R.; Yoon, Y. J.; Yi, H.-B.; Kim, W. Y.; Kim, K. S. *J. Phys. Chem. A* **2004**, *108*, 2949. (g) Christie, R. A.; Jordan, K. D. *J. Phys. Chem. B* **2002**, *106*, 8376. (h) Mella, M.; Kuo, J.-L.; Clary, D. C.; Klein, M. L. *Phys. Chem. Chem. Phys.* **2005**, *7*, 2324. (i) Svanberg, M; Pettersson, J. B. C. *J. Phys. Chem. A* **1998**, *102*, 1865. (j) Shin, I.; Park, M.; Min, S. K.; Lee, E. C.; Suh, S. B.; Kim, K. S. *J. Chem. Phys.* **2006**, *125*, 234305. (k) Newton, M. D.; Ehrenson, S. *J. Am. Chem. Soc.* **1971**, *93*, 4971. (l) Dai, J.; Zlatko, B.; Huang, X.; Carter, S.; Bowman, J. M. *J. Chem. Phys.* **2003**, *119*, 6571.

(4) Singh, N. J.; Park, M.; Min, S. K.; Suh, S. B.; Kim, K. S. *Angew. Chem., Int. Ed.* **2006**, *45*, 3795; *Angew. Chem.* **2006**, *118*, 3879.

(5) (a) Headrick, J. M.; Diken, E. G.; Walters, R. S.; Hammer, N. I.; Christie, R. A.; Cui, J.; Myshakin, E. M.; Duncan, M. A.; Johnson, M. A.; Jordan, K. D. *Science* **2005**, *308*, 1765. (b) Headrick, J. M.; Bopp, J. C.; Johnson, M. A. *J. Chem. Phys*. **2004**, *121*, 11523. (c) Hammer, N. I.; Diken, E. G.; Roscioli, J. R.; Johnson, M. A.; Myshakin, E. M.; Jordan, K. D.; McCoy, A. B.; Huang, X.; Bowman, J. M.; Carter, S. *J. Chem. Phys.* **2005**, *122*, 244301.

(6) Asmis, K. N.; Pivonka, N. L.; Santambrogio, G.; Brümmer, M.; Kaposta, C.; Neumark, D. M.; Wöste, L. *Science* **2003**, *299*, 1375.

(7) Fridgen, T. D.; McMahon, T. B.; MacAleese, L.; Lemaire, J.; Maitre, P. *J. Phys. Chem. A* **2004**, *108*, 9008.

(8) (a) Jiang, J.-C.; Wang, Y.-S.; Chang, H.-C.; Lin, S. H.; Lee, Y. T.; Niedner-Schatteburg, G.; Chang, H.-C. *J. Am. Chem. Soc.* **2000**, *122*, 1398. (b) Yeh, L. I.; Okumura, M. J.; Myers, J. D.; Price, J. M.; Lee, Y. T. *J. Chem. Phys*. **1989**, *91*, 7319. (c) Okumura, M. J.; Yeh, L. I.; Myers, J. D.; Lee, Y. T. *J. Chem. Phys*. **1990**, *94*, 3416. (d) Schwartz, H. A. *J. Chem. Phys*. **1977**, *67*, 1977.

(9) (a) Miyazaki, M.; Fujii, A.; Ebata, T.; Mikami, N. *Science* **2004**, *304*, 1134. (b) Shin, J. W.; Hammer, N. I.; Diken, E. G.; Johnson, M. A.; Walters, R. S.; Jaeger, T. D.; Duncan, M. A.; Christie, R. A.; Jordan, K. D. *Science* **2004**, *304*, 1140. (c) Wu, C.-C.; Lin, C.-K.; Chang, H.-C.; Jiang, J.-C.; Kuo, J.-L.; Klein, M. L. *J. Chem. Phys.* **2005**, *122*, 074315.

(10) (a) Brutschy, B. *Chem. Rev.* **2000**, *100*, 3891. (b) Buck, U.; Huisken, F. *Chem. Rev.* **2000**, *100*, 3863. (c) Kim, K. S.; Tarakeshwar, P.; Lee, J. Y. *Chem. Rev.* **2000**, *100*, 4145. (d) Kim, J.; Kim, K. S. *J. Chem. Phys*. **1998**, *109*, 5886. (e) Lee, H. M.; Suh, S. B.; Lee, J. Y.; Tarakeshwar, P.; Kim, K. S. *J. Chem. Phys.* **2000**, *112*, 9759. (f) Hammer, N. I.; Shin, J. W.; Headrick, J. M.; Diken, E. G.; Roscioli, J. R.; Weddle, G. H.; Johnson, M. A. *Science*, **2004**, *306*, 675. (g) Patwari, G. N.; Lisy, J. M. *J. Chem. Phys.* **2003**, *118*, 8555.

(11) Hütter, J.; Alavi, A.; Deutsch, T.; Bernasconi, M.; Focher, P.; Fois, E.; Goedecker, S.; Marx, D.; Tuckerman, M.; Parinello, M. et al. *CPMD* version 3.9.2; IBM Research Division, MPI Festkoerperforschung: Stuttgart, Germany, 1990−2005.

(12) Eigen, M. *Angew. Chem. Int. Ed.* **1964**, *3*, 1.

(13) Zundel, G.; Metzer, H. *Z. Phys. Chem.* **1968**, *58*, 225.

(14) (a) Becke, A. D. *Phys. Rev. A: At., Mos., Opt. Phys* **1988**, *38*, 3098. (b) Lee, C.; Yang, W.; Parr, R G. *Phys. Rev. B: Condens. Mater*. **1988**, *37*, 785.

(15) Frisch, M. J.; Trucks, G. W.; Schlegel, H. B.; Scuseria, G. E.; Robb, M. A.; Cheeseman, J. R.; Montgomery, J. A., Jr.; Vreven, T.; Kudin, K. N.; Burant, J. C.; Millam, J. M.; Iyengar, S. S.; Tomasi, J.; Barone, V.; Mennucci, B.; Cossi, M.; Scalmani, G.; Rega, N.; Petersson, G. A.; Nakatsuji, H.; Hada, M.; Ehara, M.; Toyota, K.; Fukuda, R.; Hasegawa, J.; Ishida, M.; Nakajima, T.; Honda, Y.; Kitao, O.; Nakai, H.; Klene, M.; Li, X.; Knox, J. E.; Hratchian, H. P.; Cross, J. B.; Bakken, V.; Adamo, C.; Jaramillo, J.; Gomperts, R.; Stratmann, R. E.; Yazyev, O.; Austin, A. J.; Cammi, R.; Pomelli, C.; Ochterski, J. W.; Ayala, P. Y.; Morokuma, K.; Voth, G. A.; Salvador, P.; Dannenberg, J. J.; Zakrzewski, V. G.; Dapprich, S.; Daniels, A. D.; Strain, M. C.; Farkas, O.; Malick, D. K.; Rabuck, A. D.; Raghavachari, K.; Foresman, J. B.; Ortiz, J. V.; Cui, Q.; Baboul, A. G.; Clifford, S.; Cioslowski, J.; Stefanov, B. B.; Liu, G.; Liashenko, A.; Piskorz, P.; Komaromi, I.; Martin, R. L.; Fox, D. J.; Keith, T.; Al-Laham, M. A.; Peng, C. Y.; Nanayakkara, A.; Challacombe, M.; Gill, P. M. W.; Johnson, B.; Chen, W.; Wong, M. W.; Gonzalez, C.; Pople, J. A. *Gaussian 03*, revision B.1; Gaussian, Inc.: Wallingford, CT, 2004.

(16) Chanban, G. M.; Jung, J. O.; Gerber, R. B. *J. Chem. Phys.* **1999**, *111*, 1823.

(17) Werner, H.-J.; Knowles, P. J.; Amos, R. D.; Bernhardsson, A.; Berning, A.; Celani, P.; Cooper, D. L.; Deegan, M. J. O.; Dobbyn, A. J.; Eckert, F.; Hampel, C.; Hetzer, G.; Korona, T.; Lindh, R.; Lloyd, A. W.; McNicholas, S. J.; Manby, F. R.; Meyer, W.; Mura, M. E.; Nicklass, A.; Palmieri, P.; Pitzer, R.; Rauhut, G.; Schütz, M.; Schumann, U.; Stoll, H.; Stone, A. J.; Tarroni, R.; Thorsteinsson, T. *MOLPRO*, 2002.6; University of Birmingham: Birmingham, England, 2002.

(18) Lee, S. J.; Chung, H. Y.; Kim, K. S. *Bull. Korean Chem. Soc.* **2004**, *25*, 1061.

(19) Martyna, G. J.; Tuckerman, M. E. *J. Chem. Phys.* **1999**, *110*, 2810.

(20) (a) Trouiller, N.; Martins, J. L. *Phys. Rev. B: Condens. Mater*. **1991**, *43*, 1993. (b) Sprik, M.; Hutter, J.; Parrinello, M. *J. Chem. Phys.* **1996**, *105*, 1142.

(21) Nos'e, S. *J. Chem. Phys*. **1984**, *81*, 511(b) Nos'e, S. *Mol. Phys*. **1984**, *52*, 255. (c) Hoover, W. G. *Phys. Rev. A: At., Mos., Opt. Phys.* **1985**, *31*, 1695.

(22) Odutola, J. A.; Dyke, T. R. *J. Chem. Phys.* **1980**, *72*, 5062. (b) Kim, K. S.; Mhin, B. J.; Choi, U-S.; Lee, K. *J. Chem. Phys.* **1992**, *97*, 6649. (c) Lee, H. M.; Suh, S. B.; Lee, J. Y.; Tarakeshwar, P.; Kim, K. S. *J. Chem. Phys.* **2000**, *112*, 9759.

(23) Benedict, W. S.; Gailar, N.; Plyler, E. K. *J. Chem. Phys.* **1956**, *24*, 1139.

(24) Gaigeot, M. P.; Vuilleumier, R.; Sprik, M.; Borgis, D. *J. Chem. Theory Comput.* **2005**, *1*, 772.

(25) (a) Begemann, M. H.; Gudeman, C. S.; Pfaff, J.; Saykally, R. J. *Phys. Rev. Lett.* **1983**, *51*, 554. (b) Tang, J.; Oka, T. *J. Mol. Spectrosc.* **1999**, *196*, 120. (c) Gruebele, M.; Polak, M.; Saykally, R. J. *J. Chem. Phys.* **1987**, *87*, 3347. (d) Liu, D.-J.; Haese, N. N.; Oka, T. *J. Chem. Phys*. **1985**, *82*, 5368.

(26) (a) Xie, Y.; Remington, R. B.; Schaefer, H. F., III. *J. Chem. Phys.* **1994**, *101*, 4878. (b) Valeev, E. F.; Schaefer, H. F., III. *J. Chem. Phys.* **1998**, *108*, 7197. (c) Klein, S.; Kochanski, E.; Strich, A.; Sadlej, A. J. *J. Phys. Chem. A* **1997**, *101*, 4799. (d) Huang, X.; Cho, H. M.; Carter, S.; Ojamae, L.; Bowman, J. M.; Singer, S. J. *J. Phys. Chem. A* **2003**, *107*, 7142. (e) Verner, M. V.; Kuhn, O.; Sauer, J. *J. Chem. Phys.* **2001**, *114*,

240. (f) Cho, H. M.; Singer, S. J. *J. Phys. Chem. A* **2004**, *108*, 8691. (g) Sauer, J.; Dobler, J. *ChemPhysChem.* **2005**, *6*, 1706. (h) Dai, J.; Bacic, Z.; Huang, X.; Carter, S.; Bowman, J. M. *J. Chem. Phys.* **2003**, *119*, 6571. (i) Kaledin, M.; Kaledin, A. L.; Bowman, J. M. *J. Phys. Chem. A* **2006**, *110*, 2933. (j) Cheng, H.-P.; Krause, J. L. *J. Chem. Phys.* **1997**, *107*, 8461. (k) Cheng, H.-P. *J. Phys. Chem.* **1998**, *102*, 6201.

(27) Kim, J.; Lee, H. M.; Suh, S. B.; Majumdar, D.; Kim, K. S. *J. Chem. Phys.* **2000**, *113*, 5259.